 Related Commentary, page 3102

Induced pluripotent stem cell–derived hepatocytes have the functional and proliferative capabilities needed for liver regeneration in mice

Silvia Espejel,[1,2] Garrett R. Roll,[2] K. John McLaughlin,[3] Andrew Y. Lee,[1] Jenny Y. Zhang,[1] Diana J. Laird,[1,4] Keisuke Okita,[5] Shinya Yamanaka,[5,6] and Holger Willenbring[1,2]

[1]Eli and Edythe Broad Center for Regeneration Medicine and Stem Cell Research and [2]Department of Surgery, Division of Transplantation, University of California San Francisco, San Francisco, California, USA. [3]Center for Molecular and Human Genetics, The Research Institute at Nationwide Children's Hospital, Columbus, Ohio, USA. [4]Department of Obstetrics, Gynecology and Reproductive Sciences, University of California San Francisco, San Francisco, California, USA. [5]Center for iPS Cell Research and Application, Institute for Integrated Cell-Material Sciences, Kyoto University, Kyoto, Japan. [6]Gladstone Institute of Cardiovascular Disease, San Francisco, California, USA.

The ability to generate induced pluripotent stem (iPS) cells from a patient's somatic cells has provided a foundation for organ regeneration without the need for immune suppression. However, it has not been established that the differentiated progeny of iPS cells can effectively reverse failure of a vital organ. Here, we examined whether iPS cell–derived hepatocytes have both the functional and proliferative capabilities needed for liver regeneration in mice with fumarylacetoacetate hydrolase deficiency. To avoid biases resulting from random genomic integration, we used iPS cells generated without viruses. To exclude compensation by hepatocytes not derived from iPS cells, we generated chimeric mice in which all hepatocytes were iPS cell derived. In vivo analyses showed that iPS cells were intrinsically able to differentiate into fully mature hepatocytes that provided full liver function. The iPS cell–derived hepatocytes also replicated the unique proliferative capabilities of normal hepatocytes and were able to regenerate the liver after transplantation and two-thirds partial hepatectomy. Thus, our results establish the feasibility of using iPS cells generated in a clinically acceptable fashion for rapid and stable liver regeneration.

Introduction

The discovery that overexpression of a few transcription factors suffices to reprogram somatic cells to pluripotency has paved the way for organ regeneration with autologous cells not requiring immune suppression (1). Further progress toward the clinic was recently made by generating induced pluripotent stem (iPS) cells free of viral vector and transgene sequences, a process which prevents potential hazards from mutagenesis or persistent pluripotent gene expression (2). The first evidence for the therapeutic potential of iPS cells has come from studies of the effects of iPS cell–derived hematopoietic cells, neurons, or endothelial cells in animal models of human diseases (3–5). However, whether the differentiated progeny of iPS cells are capable of regenerating a failing vital organ remains to be determined.

The liver is a vital organ that represents a promising target for cell therapy, because of its ability to functionally integrate transplanted hepatocytes. Pioneering trials in patients and studies in animal models have revealed that successful liver regeneration requires that transplanted cells have both the complex functional and unique proliferative capabilities of fully differentiated hepatocytes (6, 7). Otherwise, replacing approximately 20% or 1×10^{10} of the hepatocytes in the liver, as is required for restoration of liver function in most human liver diseases, can neither be achieved nor sustained (8).

It has recently been shown, using tetraploid embryo complementation, that iPS cells can develop into all cell types in mice (9–11). However, it is unknown whether iPS cell–derived hepatocytes have the same functional output as normal adult hepatocytes and share their ability to respond to injury by rapidly entering the cell cycle and proliferating extensively. In fact, recent reports have challenged the therapeutic potential of iPS cells by showing that they differentiate and proliferate less efficiently than ES cells (12, 13).

Here, we aimed at defining the effectiveness of iPS cells in organ regeneration by investigating the functional and proliferative capabilities of iPS cell–derived hepatocytes. To exclude biases due to viral genomic integration or persistent pluripotent gene expression, we used iPS cells free of foreign DNA (14). Instead of tetraploid embryo complementation, which is inefficient and has yet to be achieved with iPS cells free of foreign DNA, we used blastocysts deficient in fumarylacetoacetate hydrolase (FAH) to generate chimeric mice in which progressive liver repopulation with iPS cell–derived hepatocytes could be induced postnatally. Since the entire liver was composed of iPS cell–derived hepatocytes by the time the mice reached adulthood, we were able to analyze the level of liver function and the efficacy of liver regeneration afforded by differentiated iPS cell–derived hepatocytes in the absence of compensation by non–iPS cell–derived hepatocytes.

Results

FAH-deficient blastocysts as a tool to define the therapeutic potential of iPS cell–derived hepatocytes. Genetic deficiency of FAH, a tyrosine-degrad-

Authorship note: Silvia Espejel and Garrett R. Roll contributed equally to this work.
Conflict of interest: The authors have declared that no conflict of interest exists.
Citation for this article: *J Clin Invest.* 2010;120(9):3120–3126. doi:10.1172/JCI43267.

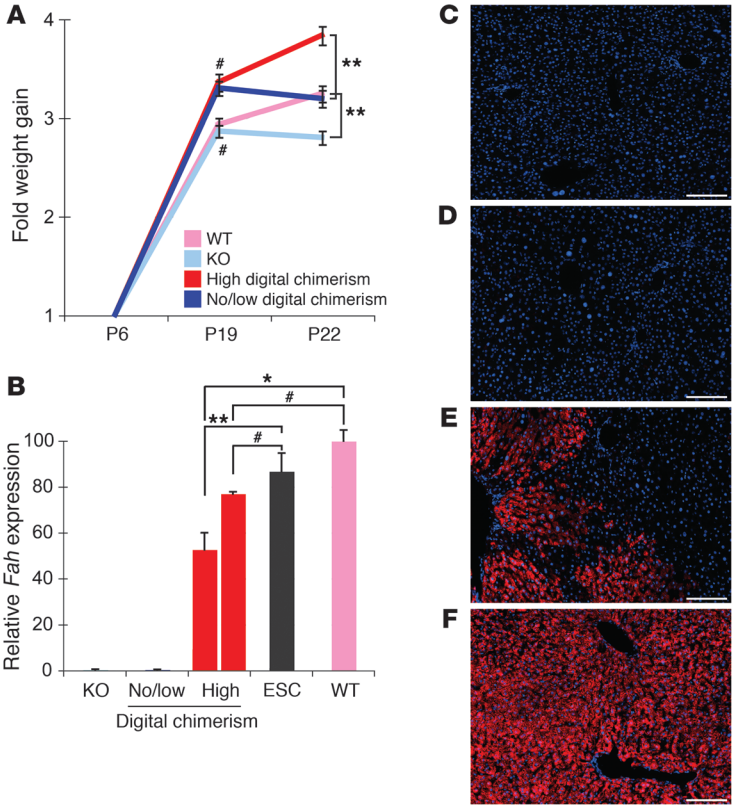

Figure 1

iPS cell–derived hepatocytes facilitate NTBC-independent growth and survival of FAH-deficient mice. (**A**) Relative postnatal weight gain in chimeric mice compared with wild-type and FAH-deficient (KO) controls. Chimeric mice were separated into 2 groups, based on high versus no/low contribution of iPS cells to genomic DNA from digits (Supplemental Figure 1). NTBC withdrawal was initiated on P6. In contrast to KO controls and mice with no/low levels of digital chimerism, mice with high levels of digital chimerism did not require reinstatement of NTBC treatment after P22 for growth and survival. All control mice were on the 129S4 strain background, while both iPS cells and blastocysts were on a mixed 129S4 and C57BL/6 background. C57BL/6 neonates grow faster, which explains the slight difference in weight gain between control and chimeric mice between P6 and P19. (**B**) Quantitative RT-PCR shows that growth and survival in the absence of NTBC are strictly correlated with *Fah* expression in the liver. Liver *Fah* expression is detectable in all mice with a high iPS cell contribution to digits but not in mice with no/low levels of digital chimerism. *Fah* expression approaches wild-type levels with time off NTBC, increasing from approximately 50% (range, 33%–69%) in mice analyzed at P28 (left red bar) to approximately 80% (range, 76%–78%) in mice analyzed at P70 (right red bar). Maximum *Fah* expression levels in iPS cell chimeric mice are similar to levels found after approximately 100% liver repopulation in mice generated by injection of normal ES cells into FAH-deficient blastocysts (ESCs). (**C**–**F**) FAH immunostaining (red). Representative liver sections show that mice with (**C**) no or (**D**) low digital chimerism lack FAH-expressing cells. Livers of mice with high levels of digital chimerism show repopulation with FAH-positive cells, between approximately (**E**) 50% at P28 and (**F**) 100% at P70. Nuclei are stained blue. Scale bars: 100 μm. Data represent mean ± SEM. $^{*}P < 0.05$; $^{**}P < 0.005$; $^{\#}P > 0.05$.

ing enzyme expressed specifically in hepatocytes in the liver, causes the liver disease tyrosinemia type I. Unless treated with the drug 2-(2-nitro-4-fluoromethylbenzoyl)-1,3-cyclohexanedione (NTBC), many humans and all mice lacking FAH develop severe hepatocyte damage and die from liver failure in the neonatal period (15). The liver injury caused by FAH deficiency confers a selective growth advantage on wild-type hepatocytes. Because hepatocytes have stem cell–like proliferative capabilities, a relatively small number of transplanted wild-type hepatocytes can completely repopulate the FAH-deficient liver (7). However, only cells that have the same functional and proliferative capabilities as normal adult hepatocytes are effective in liver repopulation. Cells that exhibit incomplete differentiation and impaired proliferation, a prominent example being hepatocyte-like cells generated from ES cells with current in vitro differentiation protocols, fail to restore liver function in FAH-deficient mice or similar liver repopulation models (16–18).

To definitely determine the regenerative capabilities of iPS cell–derived hepatocytes, we decided to subject these cells to the rigorous testing of hepatocyte function and proliferation afforded by the FAH-deficient liver, while avoiding the limitations of current in vitro differentiation protocols. To achieve this, we generated chimeric mice by injection of iPS cells into blastocysts obtained from FAH-deficient mice. As an example of iPS cells free of foreign DNA, we used the iPS cell line 440A-3 that was generated by repeated transfection of mouse embryonic fibroblasts with plasmids expressing *Oct4*, *Sox2*, *Klf4*, and *c-Myc* (14). To obtain neonates with a stochastic contribution of iPS cells to all tissues, we matched the mouse strain background of the iPS cells and the blastocysts. Moreover, we treated the foster mothers carrying the iPS cell–injected blastocysts with NTBC to prevent damage to FAH-deficient hepatocytes and maintain the stochastic liver chimerism until initiation of NTBC withdrawal after birth (15).

After transfer of 40 iPS cell–injected, FAH-deficient blastocysts into foster mothers, a total of 24 pups were born. In 8 of these mice, we found that iPS cells contributed to the tissues making up the digits (Supplemental Figure 1; supplemental material available online with this article; doi:10.1172/JCI43267DS1). To investigate whether the livers of these pups or the 16 neonates without chimerism in digits (referred to herein as digital chimerism) harbored iPS cell–derived hepatocytes and whether their functional and proliferative capabilities sufficed to restore liver function, we deprived the foster mothers of NTBC by gradually lowering its concentration in the drinking water (15). In the absence of NTBC from the breast milk, the 6 neonates with high levels of digital chimerism continued to thrive, while the remaining 18 neonates lost weight and NTBC treatment had to be reinstated to prevent death (Figure 1A). Similarly, pups derived from FAH-deficient blastocysts that were not injected with iPS cells rapidly deteriorated and required rescue from liver failure with NTBC (Figure 1A).

iPS cell–derived hepatocytes provide normal liver function. Next, we asked whether NTBC-independent survival from FAH deficiency was due to the presence of iPS cell–derived hepatocytes. We found no evidence for *Fah* gene or protein expression in liver tissue samples obtained from mice with no or low levels of digital chimerism at P28 or P70 (Figure 1, B–D). This was not due to impaired differentiation of iPS cells, because genomic DNA isolated from the livers of these mice contained only the knockout *Fah* allele (data not shown). This shows

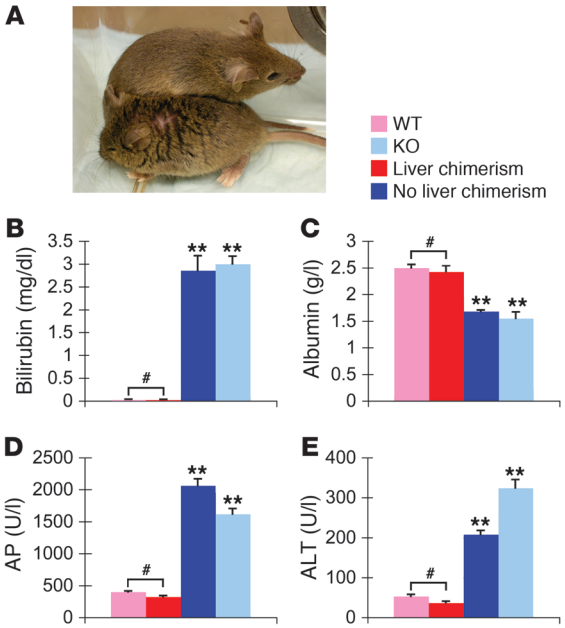

Figure 2
Restoration of liver function in FAH-deficient mice repopulated with iPS cell–derived hepatocytes. (**A**) In the absence of NTBC, a mouse with no digital chimerism is lethargic and shows signs of dehydration and lack of grooming (front), while a littermate with high levels of digital chimerism appears normal (back) at P22. (**B**–**E**) Blood analysis of liver function parameters at P22 in mice deprived of NTBC since P6. (**B**) Bilirubin and (**C**) albumin levels reflect the detoxification and protein synthesis functions of the liver, respectively. (**D**) Alkaline phosphatase (AP) is a marker of cholestasis, (**E**) while alanine aminotransferase (ALT) indicates hepatocyte injury. Mice with iPS cell contribution to the liver (all mice with high levels of digital chimerism, referred to as liver chimerism) have values indistinguishable from wild-type mice (including undetectable bilirubin), while the results from mice with no liver chimerism (all mice with no/low levels of digital chimerism) and FAH-deficient mice indicate liver failure. Liver function parameters of the mice with liver chimerism were stable at reanalysis at P70 and P300 (Supplemental Figure 2). Data represent mean ± SEM. $^{**}P < 0.005$; $^{\#}P > 0.05$.

that iPS cell contribution can vary between individual organs in chimeric mice. In contrast to mice with no or low levels of digital chimerism, mice with high levels of digital chimerism showed various levels of liver repopulation with FAH-expressing hepatocytes, ranging from approximately 50% repopulation at P28 (Figure 1E) to approximately 100% repopulation at P70 (Figure 1F). The extent of liver repopulation observed in tissue sections correlated with *Fah* gene expression levels in samples representative of the whole liver. Mice fully repopulated with iPS cell–derived hepatocytes produced approximately 80% of the *Fah* transcription of wild-type mice (Figure 1, B and F). We found similar *Fah* expression levels in livers of chimeric mice fully repopulated with hepatocytes derived from ES cells, suggesting that iPS cell–derived hepatocytes are fully differentiated (Figure 1B).

As direct evidence for the functional capabilities of hepatocytes derived from iPS cells, we found that liver repopulation with these cells led to complete restoration of liver function by P22 (Figure 2). The less than 50% liver repopulation at this time suggested that the functional output and ability to rescue liver function of iPS cell–derived hepatocytes are similar to those of normal hepatocytes. Indeed, despite continued NTBC withdrawal, mice with high levels of digital chimerism grew and had completely normal liver function parameters at P70, when approximately 100% of the hepatocytes were of iPS cell origin (Supplemental Figure 2). Liver function tests continued to be normal at P300, that is after 10 months of NTBC withdrawal (Supplemental Figure 2). As additional evidence for normal hepatocyte differentiation, iPS cell–derived hepatocytes normalized plasma amino acid levels (Supplemental Table 1) and underwent physiological polyploidization (Supplemental Figure 3). In the absence of compensation by non–iPS cell–derived hepatocytes, these results show that iPS cells can give rise to hepatocytes that are fully and stably differentiated.

iPS cell–derived hepatocytes and renal proximal tubular cells replicate the unique proliferative capabilities of their wild-type equivalents. Levels of liver repopulation progressed from predominantly approximately 50% at P28 to invariably approximately 100% at P70 (Figure 1, E and F). Since we initiated NTBC withdrawal at P6, this finding indicates that the number of iPS cell–derived hepatocytes present at birth was small and that these cells continuously proliferated to form small nodules by P28 and achieve approximately 100% liver repopulation by P70. Indeed, we found that cells in the periphery of the nodules present in chimeric mice at P28 expressed both the hepatocyte-specific protein FAH and the pan-proliferation marker Ki67 (Figure 3A). Since final hepatocyte number and differentiation are established by P21 in mice, these observations suggest that differentiated iPS cell–derived hepatocytes responded to FAH deficiency by dividing until all FAH–deficient hepatocytes were replaced (7).

In addition to hepatocytes, FAH is expressed in proximal tubular cells of the kidney, and its deficiency causes tubulopathy (15). Correction of liver function improves tubular function by restoring liver tyrosine catabolism (19). Therefore, we analyzed plasma creatinine and urine amino acid levels in the chimeric mice to further define the functional capabilities of iPS cell–derived hepatocytes (for details see Supplemental Methods). Since mild tubulopathy persists in FAH deficiency even after whole organ liver transplantation (19), we were surprised to find not only normal creatinine excretion but also normal reabsorption of urine amino acids (Supplemental Figure 4 and Supplemental Table 2). Considering that normal proximal tubular cells are positively selected in FAH-deficient kidneys (20), we asked whether iPS cell–derived proximal tubular cells had regenerated the kidneys of the chimeric mice. Indeed, we found substantial repopulation with iPS cell–derived proximal tubular cells (Supplemental Figure 4). Together, these findings suggest that iPS cell–derived renal proximal tubular cells provide therapeutically effective function and have the ability to proliferate extensively.

The ability of differentiated hepatocytes or renal proximal tubular cells to proliferate is an important prerequisite for both achieving and sustaining a therapeutic effect with cell therapy. To determine whether differentiated iPS cell–derived hepatocytes are effective in liver regeneration after transplantation, we isolated iPS cell–derived hepatocytes from a chimeric mouse and transplanted 1×10^6 of these cells into adult FAH-deficient mice. Similar to normal hepatocytes, iPS cell–derived hepatocytes rapidly repopulated the livers of these mice so that they became NTBC indepen-

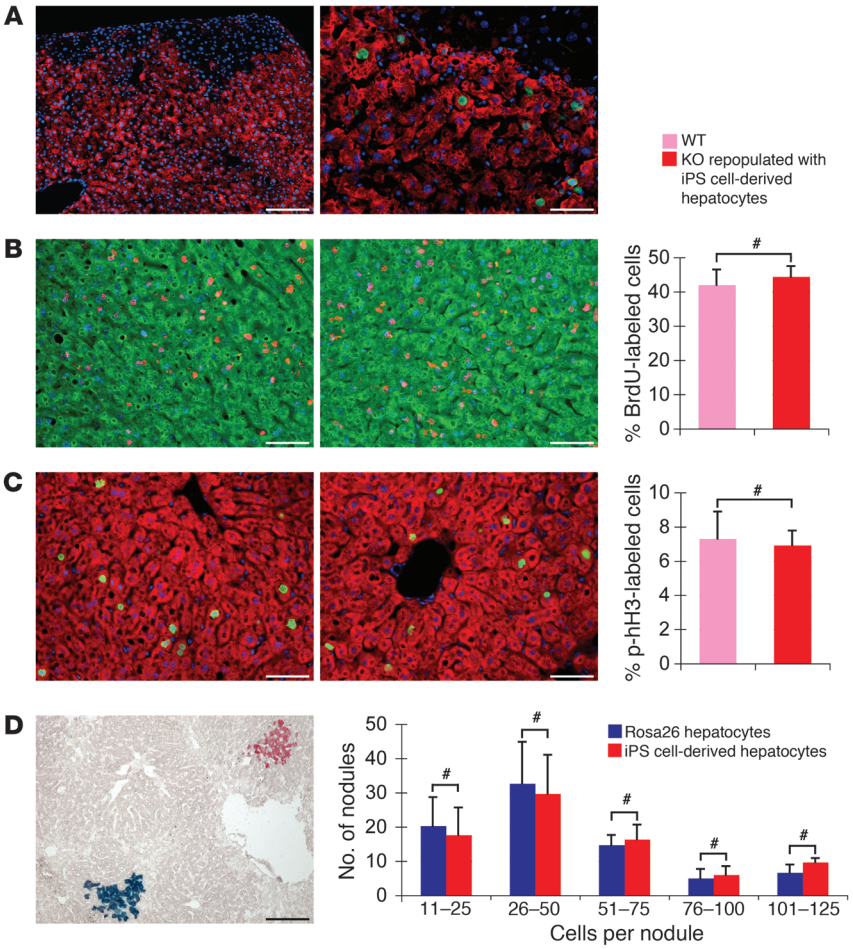

Figure 3

iPS cell–derived hepatocytes have normal proliferative capabilities. (**A**) FAH immunostaining (red, both images) shows approximately 90% liver repopulation with FAH-expressing hepatocytes in a chimeric mouse at P28. Additional Ki67 immunostaining (green, right image) shows proliferating FAH-positive hepatocytes bordering growth-arrested FAH-negative hepatocytes. (**B** and **C**) Analysis of liver regeneration after two-thirds partial hepatectomy in 3 wild-type and 3 FAH-deficient mice repopulated to approximately 100% with transplanted iPS cell–derived hepatocytes (FAH immunostaining, green or red). (**B**) BrdU labeling (red) 40 hours after two-thirds partial hepatectomy shows that timing and magnitude of DNA synthesis are indistinguishable between wild-type hepatocytes (left) and iPS cell–derived hepatocytes (middle). Quantification of BrdU-labeled hepatocytes in all mice (right). (**C**) Immunostaining for phosphorylated histone H3 (p-hH3, green) 48 hours after two-thirds partial hepatectomy shows that wild-type hepatocytes (left) and iPS cell–derived hepatocytes (middle) progress into mitosis with similar efficiency. Quantification of p-hH3–labeled hepatocytes in all mice (right). (**D**) Combined FAH immunostaining (red) and X-gal staining (blue) shows 2 nodules of similar size derived from a single iPS cell–derived hepatocyte or a Rosa26 hepatocyte transplanted together into an immune-deficient, FAH-deficient mouse. The blue X-gal staining masks the red FAH signal. Both FAH immunostaining and X-gal staining are highly sensitive and specific (Figure 1, E and F, and Supplemental Figure 6). Classifying repopulating nodules based on the number of hepatocytes visible in 2-dimensional liver sections (cells per nodule) indicates that cotransplanted Rosa26 hepatocytes and iPS cell–derived hepatocytes are equally effective in clonal expansion. The number of cell divisions required for formation of repopulating nodules composed of 11–25, 26–50, 51–75, 76–100, or 101–125 hepatocytes is 7, 8, 9, 10, or 11, respectively. This calculation is based on the assumption that each hepatocyte in the nodule proliferates to the same extent and that nodules are 3-dimensional spheres (35). Results of 3 transplantation experiments are shown. Nuclei are stained blue. Scale bars: 100 μm (**A**, left image, and **D**); 50 μm (**B** and **C**); 25 μm (**A**, right image). Data represent mean ± SEM. $^{\#}P > 0.05$.

dent (Figure 3, B and C). We then challenged livers constituted of approximately 100% of iPS cell–derived hepatocytes with two-thirds partial hepatectomy (21). Like wild-type mice and chimeric mice operated on at P28 and P70, all mice repopulated with transplanted iPS cell–derived hepatocytes tolerated two-thirds partial hepatectomy normally and survived long-term (Supplemental Figure 5 and data not shown). Moreover, we found that differentiated iPS cell–derived hepatocytes responded to two-thirds partial hepatectomy with the rapid and coordinated cell cycle entry and progression characteristic of normal liver regeneration (Figure 3, B and C).

These findings suggested that iPS cell–derived hepatocytes can proliferate as rapidly and extensively as normal hepatocytes (22). As a definitive test, we directly compared the proliferative capabilities of iPS cell–derived hepatocytes with normal hepatocytes by performing a competitive liver repopulation experiment. We mixed an equal number of hepatocytes isolated from a highly repopulated chimeric mouse and an age-matched mouse ubiquitously expressing a β-galactosidase marker gene (*Rosa26*; ref. 23) and transplanted the cells into FAH-deficient mice. We used FAH-deficient mice that were also immune-deficient to exclude biases potentially caused by the marker gene (24). Analysis of the number and size of nodules forming in response to NTBC withdrawal in the livers of these mice revealed that iPS cell–derived hepatocytes had the same ability to continuously divide as normal hepatocytes (Figure 3D). Viewed together, our results establish that fully differentiated iPS cell–derived hepatocytes have normal proliferative capabilities.

iPS cells differentiate into normal hepatocytes in the absence of cell fusion. Previously, we showed that fusion with wild-type hematopoietic cells corrects the hepatocytes of FAH-deficient mice, leading to therapeutic liver repopulation (25, 26). A recent study based on analyses in chimeric mice even suggested that hepatocyte fusion contributes to the physiological polyploidization of the liver (27). To prove that the FAH-expressing hepatocytes in iPS cell chimeras resulted from direct iPS cell differentiation and not from fusion of iPS cell progeny with blastocyst-derived hepatocytes, we determined that blastocyst-specific markers were absent in the vast majority of hepatocytes isolated from a highly repopulated chimeric mouse (Figure 4, A and B, and Supplemental Figure 7). These analyses demonstrate that iPS cells free of foreign DNA are intrinsically able to generate fully functional hepatocytes.

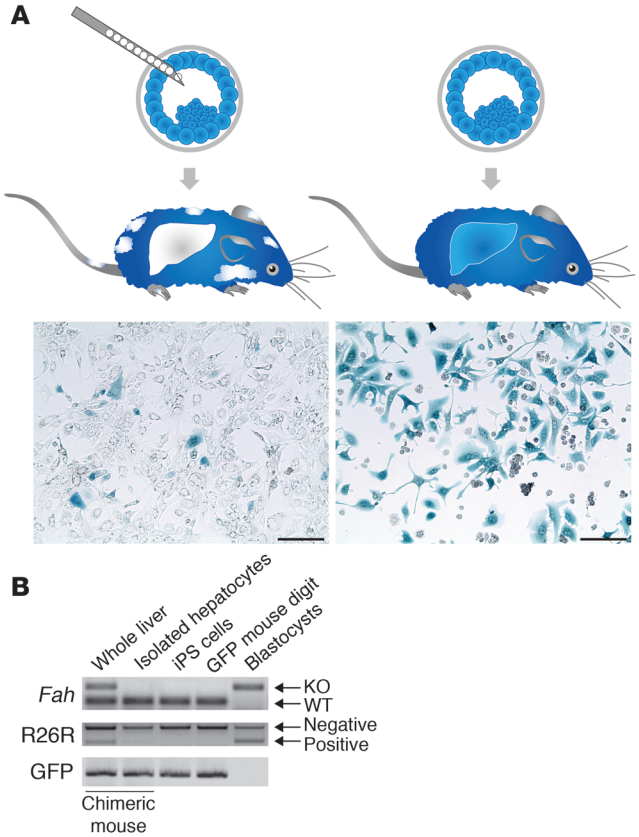

Figure 4
Differentiation of iPS cells into hepatocytes occurs in the absence of cell fusion. (**A**) Use of a ubiquitously and conditionally expressed genetic marker to exclude that iPS cells acquire hepatocyte function by fusion with blastocyst-derived hepatocytes. The FAH-deficient blastocysts used for iPS cell injection were also heterozygous for the Rosa26 reporter (R26R; ref. 32). Therefore, all cells derived from the blastocyst activate R26R (X-gal staining, blue) in response to expression of Cre recombinase. Only cells that developed by direct differentiation of the iPS cells remain unlabeled in chimeric mice. Hepatocytes isolated at approximately 95% purity from a chimeric mouse with approximately 90% liver repopulation (left) and a R26R heterozygous control mouse (right) were infected with a Cre-expressing adenovirus (Supplemental Figure 7). Activation of R26R in all hepatocytes from the R26R heterozygous mouse, but in less than 10% of the hepatocytes isolated from the chimeric mouse, shows that iPS cell–derived hepatocytes lack R26R and emerged independently of cell fusion. Scale bars: 50 μm. (**B**) Fusion-independent iPS cell differentiation into hepatocytes was confirmed by semiquantitative PCR analysis of DNA from the isolated hepatocytes for markers specific for the iPS cells (homozygous wild-type for *Fah*, homozygous negative for R26R and positive for GFP) versus markers specific for the blastocysts (homozygous knockout for *Fah*, heterozygous for R26R and negative for GFP). Due to the high level of liver repopulation in this chimeric mouse, isolated hepatocytes were predominantly iPS cell derived. A substantial fraction of the cells in the liver are not hepatocytes and are thus not replaced in response to FAH deficiency. As expected, blastocyst contribution to these cell types was maintained in the whole liver sample after NTBC withdrawal.

Discussion

In our study, after selective expansion of iPS cell–derived hepatocytes by postnatal NTBC withdrawal, all hepatocytes in the livers of adult chimeric mice were derived from iPS cells. In the absence of potential functional compensation by non–iPS cell–derived hepatocytes, our molecular and in vivo analyses established that iPS cell–derived hepatocytes are fully differentiated and that their functional output is equal to that of ES cell–derived or normal hepatocytes. Moreover, challenge by two-thirds partial hepatectomy or transplantation into adult FAH-deficient mice off NTBC showed that fibroblast origin and reprogramming did not diminish the regenerative capabilities of iPS cell–derived hepatocytes. The cells both rapidly entered the cell cycle and exhibited the extensive proliferative capabilities of normal differentiated hepatocytes.

The ability of iPS cell–derived proximal tubular cells to repopulate the kidney and correct tubulopathy extends our findings on the normal functional and proliferative capabilities of differentiated iPS cell progeny to another cell type. Recent studies showed that organ regeneration by proliferation of fully differentiated cells is not exclusive to the liver or kidney but also occurs in the pancreas (28, 29) and heart (30). Our results suggest that these proliferative capabilities could also be maintained in iPS cell–derived differentiated β cells or cardiomyocytes, which may enhance their therapeutic efficacy.

In conclusion, our results show that iPS cell–derived hepatocytes have normal functional and proliferative capabilities and are thus effective in rapidly and stably regenerating a failing liver. Since we obtained these results with iPS cells that are not subject to biases from viral genomic integration, they suggest that faithful recapitulation of hepatocyte differentiation in human iPS cells free of foreign DNA in vitro will yield an effective therapy for human liver diseases.

Methods

Mice. Procedures involving mice were approved by the Institutional Animal Care Committee at the University of California San Francisco. FAH-deficient mice on the 129S4 strain background were previously described (31). FAH-deficient mice on a pure C57BL/6 background were generated by breeding with wild-type C57BL/6 mice (The Jackson Laboratory). These animals were bred with C57BL/6 R26R mice (The Jackson Laboratory) to obtain FAH-deficient, R26R homozygous positive males for blastocyst generation. Wild-type control mice were derived from the 129S4 ES cells used to generate the original FAH-deficient mice. Thus, all control mice were on the 129S4 strain background, while the blastocysts used for iPS cell injection were F1 of 129S4 and C57BL/6 mice. Foster mothers and vasectomized males were on the ICR strain background (Taconic). Immune-deficient, FAH-deficient mice lacking B, T, and natural killer cells due to disruption of *Rag2* and *Il2rg* were on a mixed 129S4 and C57BL/6 background (24). Rosa26 mice (The Jackson Laboratory) were on a C57BL/6 background (23).

iPS and ES cell culture. The generation of the iPS cell line 440A-3 was previously described (14). The ES cells used for blastocyst injection were derived from blastocysts generated by a C57BL/6 with 129S1 mating. iPS and ES cells were cultured on confluent layers of irradiated primary mouse embryonic fibroblasts in Dulbecco's modified Eagle medium supplemented with 2 mM L-glutamine, 1% nonessential amino acids, 100 U/ml penicillin, 100 U/ml streptomycin (all Gibco, Invitrogen), 15% fetal calf serum (Hyclone), 1,000 U/ml leukemia inhibitory factor (ESGRO, Chemicon), and 0.1 mM β-mercaptoethanol (Sigma-Aldrich).

Generation of chimeric embryos. Six- to eight-week-old FAH-deficient 129S4 females were superovulated by intraperitoneal injection of 10 units of

pregnant mare's serum, followed by injection of 10 units of human chorionic gonadotropin (both Sigma-Aldrich) 48 hours later. Superovulated females were mated with FAH-deficient C57BL/6 males homozygous positive for R26R to generate blastocysts that were FAH deficient and R26R heterozygous and had the same 129S4, C57BL/6 strain background as the iPS cells (14). At 3.5 days after conception (dpc), females were killed and their oviducts and uteri were flushed with M2 medium to obtain blastocysts that, prior to iPS cell injection, were incubated in KSOM medium (both EmbryoMax, Chemicon) at 37°C and 5% CO_2. Blastocysts were injected with 10 to 15 iPS cells and transferred into the uterine horn of pseudopregnant (2.5 dpc) 6- to 8-week-old ICR mice.

Genotyping. The contribution of iPS cell–derived cells to digits and livers was determined using a PCR that simultaneously amplified the wild-type and knockout *Fah* allele in genomic DNA (31). In addition, established R26R (32) and GFP (33) PCR protocols were used to distinguish whether cells originated from the R26R heterozygous blastocyst or from the iPS cell line, 440A-3, that carries a GFP gene within the 5′ untranslated region of *Nanog* (14).

NTBC withdrawal. Foster mothers were given NTBC (7.5 mg/ml drinking water) during pregnancy. When the neonates were 6 days old, the concentration of NTBC was gradually reduced (50%, 25%, 12.5%, and 6.25%) every 2 days before drug treatment was halted. After 8 days of complete NTBC withdrawal, blood plasma was obtained by retroorbital bleeding. Body weights were recorded 0, 13, and 16 days after initiation of NTBC withdrawal. Wild-type and FAH-deficient pregnant females and neonates used as controls received the same NTBC treatment regimen. Adult immunedeficient, FAH-deficient mice were gradually taken off NTBC for 3 periods of 4 weeks, separated by 5-day-long recovery phases on NTBC.

Quantitative reverse transcription PCR. Combining samples from various regions of the liver generated a representative sample. Total RNA was isolated with TRIzol (Molecular Research Center). After DNase1 (Ambion) treatment, 1 μg RNA was used for first strand cDNA synthesis with TaqMan Reverse Transcription Reagent (Applied Biosystems). PCR was performed in a 7300 Real-Time PCR System using SYBR Green (both Applied Biosystems) at 50°C for 2 minutes and 95°C for 10 minutes, followed by 40 cycles at 95°C for 15 seconds and 60°C for 1 minute. *Fah* expression was normalized to that of *Gapdh*. Primer sequences (forward/reverse) were 5′-AGGCTTCTGCGACAATGC-3′/5′-TGCTGCCGAGAAGAGTAGAAG-3′ for *Fah* and 5′-CATGGCCTTCCGTGTTCCT-3′/5′-GCGGCACGTCAGATCCA-3′ for *Gapdh*.

Immunostaining. Liver samples were fixed at 4°C in 4% paraformaldehyde or periodate-lysine–2% paraformaldehyde (PLP) for 4 hours, cryoprotected in 30% sucrose (all Sigma-Aldrich), and embedded in optimum cutting temperature compound (Tissue-Tek, Sakura Finetek) (34). Frozen sections (10 μm) were stained with rabbit anti-FAH antibody (gift from Robert Tanguay, Université Laval, Québec City, Québec, Canada) diluted 1:15,000, rat anti-BrdU antibody (Abcam) diluted 1:100, mouse anti-Ki67 antibody (BD Pharmingen) diluted 1:25, or mouse anti-phosphorylated histone H3 antibody (Cell Signaling Technology) diluted 1:25. For fluorescence microscopy, primary antibodies were detected with goat anti-rabbit antibody conjugated with Alexa Fluor 594 or Alexa Fluor 488, goat anti-rat antibody conjugated with Alexa Fluor 594 (all Molecular Probes), diluted 1:500, and the M.O.M. Fluorescein kit (Vector). Nuclear DNA was stained with 2 μg/ml DAPI (Molecular Probes). For light microscopy, FAH immunocomplexes were detected with a swine anti-rabbit antibody conjugated with alkaline phosphatase (Dako) diluted 1:40. Alkaline phosphatase was visualized with Fast Red Substrate System (Dako).

Liver function tests. Plasma was diluted 1:4 in 0.9% sodium chloride and assayed for total bilirubin, albumin, alkaline phosphatase, and alanine aminotransferase with an ADVIA 1800 (Siemens) chemistry analyzer.

Partial hepatectomy. Two-thirds of the liver was surgically removed as described previously (21). One hundred μg/g body weight 5-bromo-2-deoxyuridine (BrdU, Roche) were injected intraperitoneally 40 hours after surgery. Immunostainings for BrdU incorporation and phosphorylation of histone H3 were performed on liver tissue obtained 48 hours after surgery.

Hepatocyte isolation. Hepatocytes were isolated from mouse liver by perfusion through a 24-gauge intraportal catheter (Surflo, Terumo) with Earle's Basic Salt Solution (EBSS, Invitrogen) plus 0.5 mM EGTA and 10 mM HEPES (both Sigma-Aldrich), followed by EBSS plus 0.1 mg/ml Liberase Blendzyme 3 (Roche). Hepatocytes were released from the liver and filtered through a 70-μm cell strainer (BD Falcon). Gravity sedimentation on ice for 30 minutes was used to enrich viable hepatocytes to approximately 95%.

Competitive liver repopulation. Hepatocytes were isolated from a highly repopulated chimeric mouse and a Rosa26 mouse, and 5×10^5 hepatocytes from each mouse were mixed and injected intrasplenically into immunedeficient, FAH-deficient mice. iPS cell–derived and Rosa26 hepatocytes were female, while recipient mice were male. Perioperative antibiotic treatment was applied as reported (24).

Adenoviral infection. An adenoviral vector expressing Cre recombinase from the cytomegalovirus promoter was obtained from the Vector Development Laboratory at Baylor College of Medicine, Houston, Texas, USA. Four hours after plating on Primaria dishes (BD Falcon), hepatocytes were incubated with the virus for 1 hour at MOIs of 4, 10, 40, and 100.

X-gal staining. Twenty-four hours after adenoviral infection, hepatocytes were fixed with 0.5% glutaraldehyde (Sigma-Aldrich). Both plated hepatocytes and PLP-fixed liver sections were exposed to 0.8 mg/ml 5-bromo-4-chloro-3-indolyl-β-D-galactopyranoside (X-gal, Sigma-Aldrich) for 12 hours at 37°C.

Estimation of hepatocytes per microscopic field. The height and width of a field was measured in pixels using Openlab software (Cellular Imaging). A standard 0.01 mm micrometer (Applied Image Inc.) was used to convert pixels to μm. The number of hepatocytes per field was estimated, assuming that a mouse hepatocyte measures 20 μm in both height and width.

Calculation of cell numbers and divisions in repopulating nodules. The number of hepatocytes present in the 2-dimensional section showing the widest diameter of a repopulating nodule was multiplied by a previously determined correction factor to estimate the total number of hepatocytes comprising the 3-dimensional nodule (35). Assuming that all hepatocytes in a nodule contribute equally to its expansion, the number of cell divisions required to reach a certain nodule size was calculated as log2 of the total number of hepatocytes per nodule.

Statistics. All statistical tests were performed with the 2-tailed Student's *t* test.

Acknowledgments

H. Willenbring received grant support from the California Institute for Regenerative Medicine, American Liver Foundation, and American Society of Transplantation; S. Espejel received support from the Cystinosis Research Foundation; G.R. Roll received support from a NRSA Hepatology Training Grant. The authors thank Alexis Bailey, Raymond Ng, Sonia Roll, and Montgomery Bissell for help with preparing the manuscript.

Received for publication April 7, 2010, and accepted in revised form June 23, 2010.

Address correspondence to: Holger Willenbring, Eli and Edythe Broad Center of Regeneration Medicine and Stem Cell Research, Department of Surgery, Division of Transplantation, University of California San Francisco, 513 Parnassus Avenue, S1457B, Campus Box 0525, San Francisco, California 94143, USA. Phone: 415.476.2417; Fax: 415.514.2346; E-mail: willenbringh@stemcell.ucsf.edu.

1. Takahashi K, Yamanaka S. Induction of pluripotent stem cells from mouse embryonic and adult fibroblast cultures by defined factors. *Cell*. 2006; 126(4):663–676.
2. O'Malley J, Woltjen K, Kaji K. New strategies to generate induced pluripotent stem cells. *Curr Opin Biotechnol*. 2009;20(5):516–521.
3. Hanna J, et al. Treatment of sickle cell anemia mouse model with iPS cells generated from autologous skin. *Science*. 2007;318(5858):1920–1923.
4. Wernig M, et al. Neurons derived from reprogrammed fibroblasts functionally integrate into the fetal brain and improve symptoms of rats with Parkinson's disease. *Proc Natl Acad Sci U S A*. 2008;105(15):5856–5861.
5. Xu D, et al. Phenotypic correction of murine hemophilia A using an iPS cell-based therapy. *Proc Natl Acad Sci U S A*. 2009;106(3):808–813.
6. Fisher RA, Strom SC. Human hepatocyte transplantation: worldwide results. *Transplantation*. 2006;82(4):441–449.
7. Overturf K, et al. Hepatocytes corrected by gene therapy are selected in vivo in a murine model of hereditary tyrosinaemia type I. *Nat Genet*. 1996; 12(3):266–273.
8. Fox IJ, Strom SC. To be or not to be: generation of hepatocytes from cells outside the liver. *Gastroenterology*. 2008;134(3):878–881.
9. Zhao XY, et al. iPS cells produce viable mice through tetraploid complementation. *Nature*. 2009; 461(7260):86–90.
10. Kang L, Wang J, Zhang Y, Kou Z, Gao S. iPS cells can support full-term development of tetraploid blastocyst-complemented embryos. *Cell Stem Cell*. 2009;5(2):135–138.
11. Boland MJ, et al. Adult mice generated from induced pluripotent stem cells. *Nature*. 2009;461(7260):91–94.
12. Hu BY, et al. Neural differentiation of human induced pluripotent stem cells follows developmental principles but with variable potency. *Proc Natl Acad Sci U S A*. 2010;107(9):4335–4340.
13. Feng Q, et al. Hemangioblastic derivatives from human induced pluripotent stem cells exhibit limited expansion and early senescence. *Stem Cells*. 2010;28(4):704–712.
14. Okita K, Nakagawa M, Hyenjong H, Ichisaka T, Yamanaka S. Generation of mouse induced pluripotent stem cells without viral vectors. *Science*. 2008;322(5903):949–953.
15. Grompe M, et al. Pharmacological correction of neonatal lethal hepatic dysfunction in a murine model of hereditary tyrosinaemia type I. *Nat Genet*. 1995;10(4):453–460.
16. Gouon-Evans V, et al. BMP-4 is required for hepatic specification of mouse embryonic stem cell-derived definitive endoderm. *Nat Biotechnol*. 2006; 24(11):1402–1411.
17. Haridass D, et al. Repopulation efficiencies of adult hepatocytes, fetal liver progenitor cells, and embryonic stem cell-derived hepatic cells in albumin-promoter-enhancer urokinase-type plasminogen activator mice. *Am J Pathol*. 2009;175(4):1483–1492.
18. Sharma AD, et al. Murine embryonic stem cell-derived hepatic progenitor cells engraft in recipient livers with limited capacity of liver tissue formation. *Cell Transplant*. 2008;17(3):313–323.
19. Pierik LJ, van Spronsen FJ, Bijleveld CM, van Dael CM. Renal function in tyrosinaemia type I after liver transplantation: a long-term follow-up. *J Inherit Metab Dis*. 2005;28(6):871–876.
20. Held PK, et al. In vivo genetic selection of renal proximal tubules. *Mol Ther*. 2006;13(1):49–58.
21. Mitchell C, Willenbring H. A reproducible and well-tolerated method for 2/3 partial hepatectomy in mice. *Nat Protoc*. 2008;3(7):1167–1170.
22. Overturf K, al-Dhalimy M, Ou CN, Finegold M, Grompe M. Serial transplantation reveals the stem-cell-like regenerative potential of adult mouse hepatocytes. *Am J Pathol*. 1997;151(5):1273–1280.
23. Zambrowicz BP, Imamoto A, Fiering S, Herzenberg LA, Kerr WG, Soriano P. Disruption of overlapping transcripts in the ROSA beta geo 26 gene trap strain leads to widespread expression of beta-galactosidase in mouse embryos and hematopoietic cells. *Proc Natl Acad Sci U S A*. 1997;94(8):3789–3794.
24. Azuma H, et al. Robust expansion of human hepatocytes in Fah(–/–)/Rag2(–/–)/Il2rg(–/–) mice. *Nat Biotechnol*. 2007;25(8):903–910.
25. Wang X, et al. Cell fusion is the principal source of bone-marrow-derived hepatocytes. *Nature*. 2003;422(6934):897–901.
26. Willenbring H, et al. Myelomonocytic cells are sufficient for therapeutic cell fusion in liver. *Nat Med*. 2004;10(7):744–748.
27. Faggioli F, Sacco MG, Susani L, Montagna C, Vezzoni P. Cell fusion is a physiological process in mouse liver. *Hepatology*. 2008;48(5):1655–1664.
28. Dor Y, Brown J, Martinez OI, Melton DA. Adult pancreatic beta-cells are formed by self-duplication rather than stem-cell differentiation. *Nature*. 2004;429(6987):41–46.
29. Teta M, Rankin MM, Long SY, Stein GM, Kushner JA. Growth and regeneration of adult beta cells does not involve specialized progenitors. *Dev Cell*. 2007;12(5):817–826.
30. Bersell K, Arab S, Haring B, Kuhn B. Neuregulin1/ErbB4 signaling induces cardiomyocyte proliferation and repair of heart injury. *Cell*. 2009; 138(2):257–270.
31. Grompe M, et al. Loss of fumarylacetoacetate hydrolase is responsible for the neonatal hepatic dysfunction phenotype of lethal albino mice. *Genes Dev*. 1993;7(12A):2298–2307.
32. Soriano P. Generalized lacZ expression with the ROSA26 Cre reporter strain. *Nat Genet*. 1999; 21(1):70–71.
33. Okabe M, Ikawa M, Kominami K, Nakanishi T, Nishimune Y. 'Green mice' as a source of ubiquitous green cells. *FEBS Lett*. 1997;407(3):313–319.
34. Bailey AS, et al. Myeloid lineage progenitors give rise to vascular endothelium. *Proc Natl Acad Sci U S A*. 2006;103(35):13156–13161.
35. Wang X, Montini E, Al-Dhalimy M, Lagasse E, Finegold M, Grompe M. Kinetics of liver repopulation after bone marrow transplantation. *Am J Pathol*. 2002;161(2):565–574.